# Synthesis of Multifunctional Metal- and Metal Oxide Core@Mesoporous Silica Shell Structures by Using a Wet Chemical Approach

## Chang Woo Kim,[a] Umapada Pal,[b] Sangji Park,[c] Jinheung Kim,[c] and Young Soo Kang*[a]

**Abstract:** We demonstrate a facile wet chemical approach for fabricating spherical metal/metal-oxide core@mesoporous silica shell hybrid nanoparticles with different core and shell thicknesses. Vertically aligned mesoporous silica (mSiO$_2$) shells were fabricated over the pre-synthesized spherical SiO$_2$ nanoparticles through a three-step strategy: 1) synthesis of core materials, 2) covering the core with an organic–inorganic composite layer, and 3) removing the organic template through calcinations in air. The mechanisms of hybrid structure formation are proposed. The multifunctional nature of the hybrid structures could be induced by incorporating guest ions/molecules, such as Ag, Mn, and TiO$_2$, into the pores of an mSiO$_2$ shell. Mn and TiO$_2$ cluster- incorporated composite structures have been tested to be antioxidizing agents and effective photocatalysts through electron spin resonance, radical scavenging tests, and the photocatalytic degradation of rhodamine B. The possibility of incorporating several hetero-element guest clusters in these mesoporous composite particles makes them highly attractive for multifunctional applications.

**Keywords:** catalyst · functionalization · host-guest molecules · mesoporous materials · radical reactions

## Introduction

Since the discovery of mesoporous silica like MCM-41 by Mobil scientists in early 1990s, the controlled synthesis of several highly ordered mesoporous MCM family members with high surface area have been reported.[1–4] These porous materials with uniform porosity and interconnected channels have shown tremendous potential for applications as catalysts,[5] inorganic filters,[6] chemical sensors,[7] nano-reactors,[8] adsorbents, and drug-releasing agents,[9] due to their fascinating selectivity.[4–12] By engineering the channel connectivity and pore network, several porous materials of unique characteristics have been fabricated for selective applications. For example, two dimensional (2-D) hexagonal channel structured MCM-41 and SBA-3 were prepared by using linear alkyl-chained surfactants. SBA-15 (prepared by Pluronic P123) has been applied for the fabrication of nanoparticles, nanowires and nanofibers.[10] Three-dimensional (3-D) networks of MCM-48 and SBA-1 could be prepared by using cetyl trimethylammonium bromide (CTAB). On the other hand, materials such as SBA-6, SBA-16, and FDU could be synthesized by using block copolymers and have been successfully applied in catalysis.[5]

Recent advances in morphology and size-controlled synthesis of mesoporous silica particles and their surface functionalization have made them suitable for internalization in plant and animal cells. These porous nanostructures functionalized with organic moieties or other nanostructures have been utilized for controlled drug release, molecular recognition, and sensing. On the other hand, several hierarchical porous silica nanostructures suitable for catalytic reactions and controlled release of therapeutic molecules have been synthesized through adequate modifications[13] of the methods by Stöber and co-workers.[14] The fabrication of micrometer and sub-micrometer sized mesoporous silica spheres,[15] solid silica spheres covered with mesoporous silica shell,[16] and magnetic nanoparticle encapsulated porous silica spheres[17] have been reported recently with promising potential in catalytic and biomedical applications. Development of such porous silica covered core@shell type architectures increases the thermal stability of the metallic or metal oxide cores that was not possible through organic surfactant capping due to deformation or aggregation of organic molecules.[18] On the other hand, a great effort has been devoted to fabricate size-controlled spherical mesoporous silica shell-covered magnetic nanoparticles,[19,20] for use as targeted drug-delivery agents. However, in most of the cases, the surface morphology and pore orientation of those

[a] C. W. Kim, Dr. Y. S. Kang
Korea Center for Artificial Photosynthesis
Department of Chemistry
Sogang University
Seoul, 121-742 (Korea)
Fax: (+82)2-701-0967
E-mail: yskang@sogang.ac.kr

[b] Dr. U. Pal
Instituto de Física, Universidad Autónoma de Puebla
Puebla 72570 (Mexico)

[c] S. Park, Dr. J. Kim
Department of Chemistry and Nano Science
Ewha Womans University
Seoul, 120–750 (Korea)

composite nanoparticles are irregular, and frequently their NOT-fully opened pores and limited shell thickness pose limitations for efficient practical applications. In general, the composite particles with micro- or nanometric cores covered with 2-D mesoporous silica reveal irregular external shapes and those covered with 3-D-channeled network exhibit polydispersity with disordered pore orientation. Moreover, these composite core@shell structures are obtained through several surface modification processes with tedious manipulations. From this morphosynthetic advantage, porous materials have been widely used as a smart support for various catalytic reactions by eminent research groups, for example, the groups of Frei,[21] Zhu and Thomas,[22] and Koodali,[23] which have dealt with the catalyst by using a porous support for resolving several problems. SBA-15-supported catalysts and functional materials have demonstrated to be more stable with enhanced catalytic activities.

In this work, we report a facile approach to synthesize metal oxide-core@mesoporous-silica shell (MO@mSiO₂) and metal-core@mesoporous-silica shell (M@mSiO₂) composite particles with varied core and shell dimensions, in which the porous channels of the meso-silica shells remain vertically oriented over the solid cores. Possibilities for utilizing these composite structures as multifunctional agents have been demonstrated through the incorporation of Ag-, Mn-, and TiO₂ nanoparticles in their porous shells. Applications of Mn- and TiO₂ nanoparticle-incorporated core–shell structures for oxidation protection of L-ascorbic acid and the photodegradation of rhodamine B have been studied. Such thickness-controlled composite particles with external pores oriented perpendicular to the core surface might be efficient candidates for utilization as catalysts and antioxidizing agents.

## Results and Discussion

Whereas most of the colloidal nanoparticles have been synthesized and manipulated by using surface stabilizer or surfactant, in which the thermal stability of the surfactant does not allow to get the proper dispersion of the nanoparticles after their removal, a silica coating over them increases their thermal stability and dispersity.[24,25] These two features were combined in our design strategy. Pre-fabricated spherical monodispersed metal oxide nanoparticles were used for covering well aligned, uniform mSiO₂ shells of different thickness. The MO@mSiO₂ hybrid spheres were prepared in three steps. First, the spherical MO core particles were synthesized through sol–gel process using well-known wet chemistry.[26,27] In the second step, a mesoporous silica shell around the MO particles was formed by using CTAB as a structure-directing agent (SDA). In the third step, the CTAB template was removed by calcinating/firing the sample in air at 600 °C for five hours. As the MO particles were synthesized in basic hydrolyzing media, inherently their surfaces were negatively charged due to the presence of oxygen or hydroxyl groups.[26,28] The electrostatic force

between the negatively charged MO surface and cationic surfactant helps to form micelles over the whole area of the MO surface facilitating direct synthesis of mSiO₂ layer of uniform thickness. The monodispersed nature of the obtained core@shell particles is favored due to the uniform size of the MO particles, which also act as the solid template for mSiO₂ shell formation. In Figure 1, the formation of the
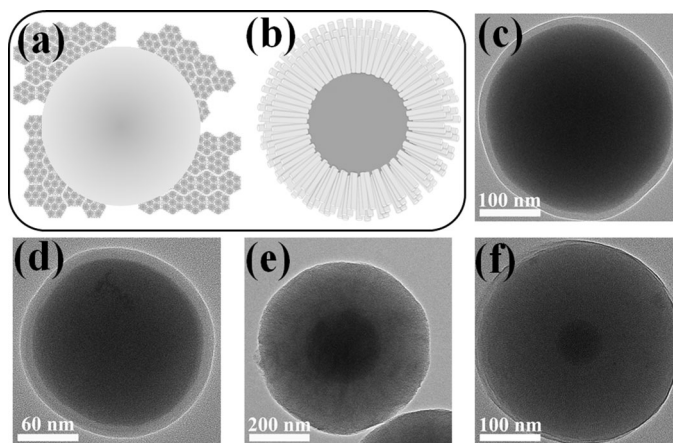


Figure 1. Schematic presentation of core particle surface with a) SDA micelles, and b) columnar meso-silica structures. Typical TEM images of SiO₂@mSiO₂ samples of c) 310 nm@14 nm, d) 163 nm@11 nm, e) 240 nm@160 nm, and f) 76 nm@126 nm.

SDA micelle and mSiO₂ shell over the MO surface have been demonstrated schematically along with the TEM images of the MO core and MO core@mSiO₂ particles. The images presented in Figure 1 illustrate the formation of MO@mSiO₂ particles with different core sizes and shell thickness.

Spherical MO cores ranging from 70 nm to 1 μm diameter could be covered with mSiO₂ shells of 126 to 11 nm in thickness. Whereas the size of the MO core could be varied during their synthesis, the width of the mSiO₂ shell could be manipulated by varying the concentrations of MO precursor and CTAB during the sol–gel process in step 2. It is noted that the size dispersion of the core@shell structures is high when the MO core diameter is smaller than 75 nm and uniform shell width is difficult to obtain for very thin shells through the sol–gel process proposed by Stöber and co-workers[14]. For core sizes that are larger than the thickness of the shell, the mesoporous channels orient themselves perpendicular to the core surface, as has been demonstrated in Figure 1 and Figure 2. The meso-shells could also be formed accommodating more than one core particle (Figure 2 and the Supporting Information) when the silica shells of larger thickness were attempted to form over smaller MO particles. The effect is prominent for the smaller MO core particles due to their higher surface energy that leads to their agglomeration. The effect has also been observed for small Pd, Au, hematite, and magnetite particles, when they were incorporated into or encapsulated by SiO₂.[21,29] By using the same synthesis protocol, various core materials were em-
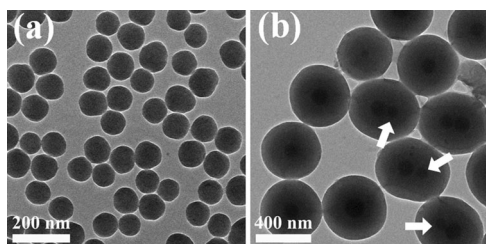
Figure 2. TEM images of a) pre-synthesized SiO₂ particles of 95 nm average diameter, and b) SiO₂@mSiO₂ structures of 95 nm@170 nm. Encapsulation of more than one silica core by the meso-silica layer can be seen in some structures due to small core size.

ployed for fabricating the hybrid core@meso-shell structures.

Figure 3 shows some typical low and high resolution TEM images of SiO₂@mSiO₂ with 337 nm@50 nm, TiO₂@mSiO₂ with 730 nm@35 nm, Ag@mSiO₂ with 191 nm@44 nm, and ZnO@mSiO₂ with 199 nm@25 nm. The TEM images highlight several important implications of the present synthesis method used to fabricate hybrid core@shell meso-structures. First, the clear formation of outer meso-shell depends on the particle dispersity in the used solvent. Core particles should be well dispersed in the reaction media for the efficient formation of meso-shell around them. The SiO₂ particles synthesized through sol–gel and Ag particles produced by chemical reduction of metal salt have good dispersity in the water/ethanol mixture solvent. A micelle of the surfac-

tant-directing agent surrounds each core particle dispersed in the solvent through electrodispersion. In comparison with SiO₂ and Ag core particles, the dispersity of TiO₂ particles in the water/ethanol mixture solvent is low, and the micelle (CTAB) frequently interacts with the surface of the partially aggregated TiO₂ particles. Second, for the formation of the mSiO₂ shell over the core particles, the reaction should be performed at pH > 11; a high pH value of the reaction mixture can frequently damage the surface of the pH-sensitive core particles, altering their morphologies. As can be seen from the Figure 3 d and Figure 4, under such basic condition,



Figure 4. Schematic presentation of mSiO₂ formation process in various MO surfaces, based on TEM images presented in Figures 2 and 3.
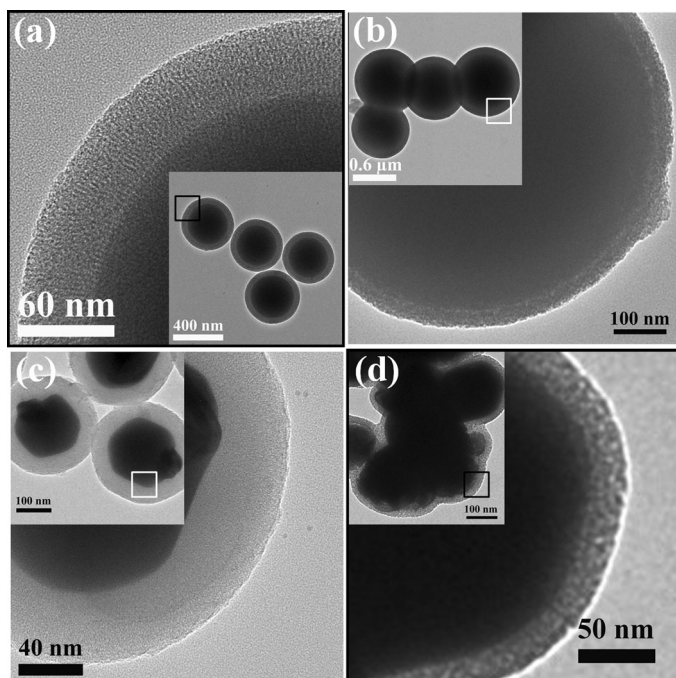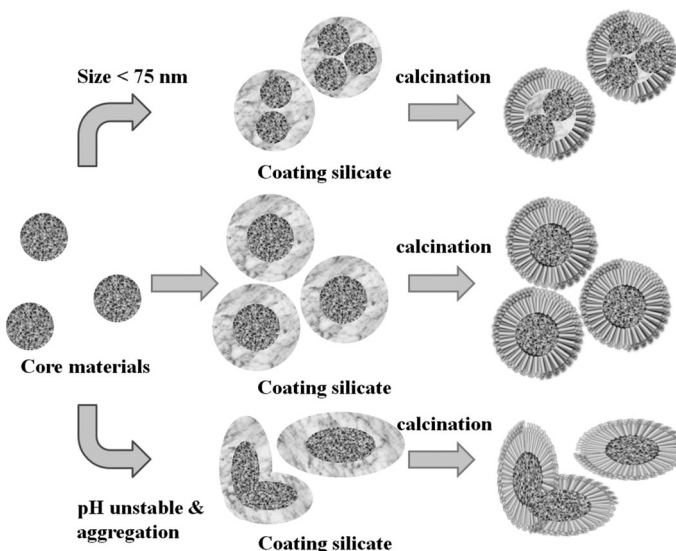


Figure 3. Typical low and high resolution TEM images of a) SiO₂@mSiO₂ of 337 nm@50 nm, b) TiO₂@mSiO₂ of 730 nm@35 nm, c) Ag@mSiO₂ of 191 nm@44 nm, and (d) ZnO@mSiO₂ of 199 nm@25 nm. Formation of the meso-silica layer with pores perpendicular to the core surface can be seen.

the shape of the ZnO particles was distorted and they were partially aggregated, indicating their limitations for using as core material in such highly basic chemical process. However, as can be seen, despite these limitations the meso-shells could be formed over the surface of metallic- and metal oxide core particles. It is expected that the meso-shell formation over other type of nanoparticles is also possible by manipulating the reaction conditions. The process of formation of meso-silica shells over pH stable and pH unstable core particles have been illustrated schematically in Figure 4.

Figure 5 presents the small-angle X-ray diffraction (SAXS) patterns and N₂ adsorption/desorption isotherms of hybrid core@shell meso-structures. There appeared no diffraction peak in the wide-angle X-ray diffraction (WAXD) of the as-prepared SiO₂ or as-prepared SiO₂@mSiO₂ samples due to their amorphous nature. The SAXS pattern of the SiO₂@mSiO₂ particles presented in Figure 5a clearly demonstrates the formation of mesoporous SiO₂ shell over the SiO₂ particles. It revealed a first order and two higher-order diffraction peaks correspond to the interplanar spacing (*d*) of 3.97, 2.27 and 1.97 nm of the ordered meso-silica shell
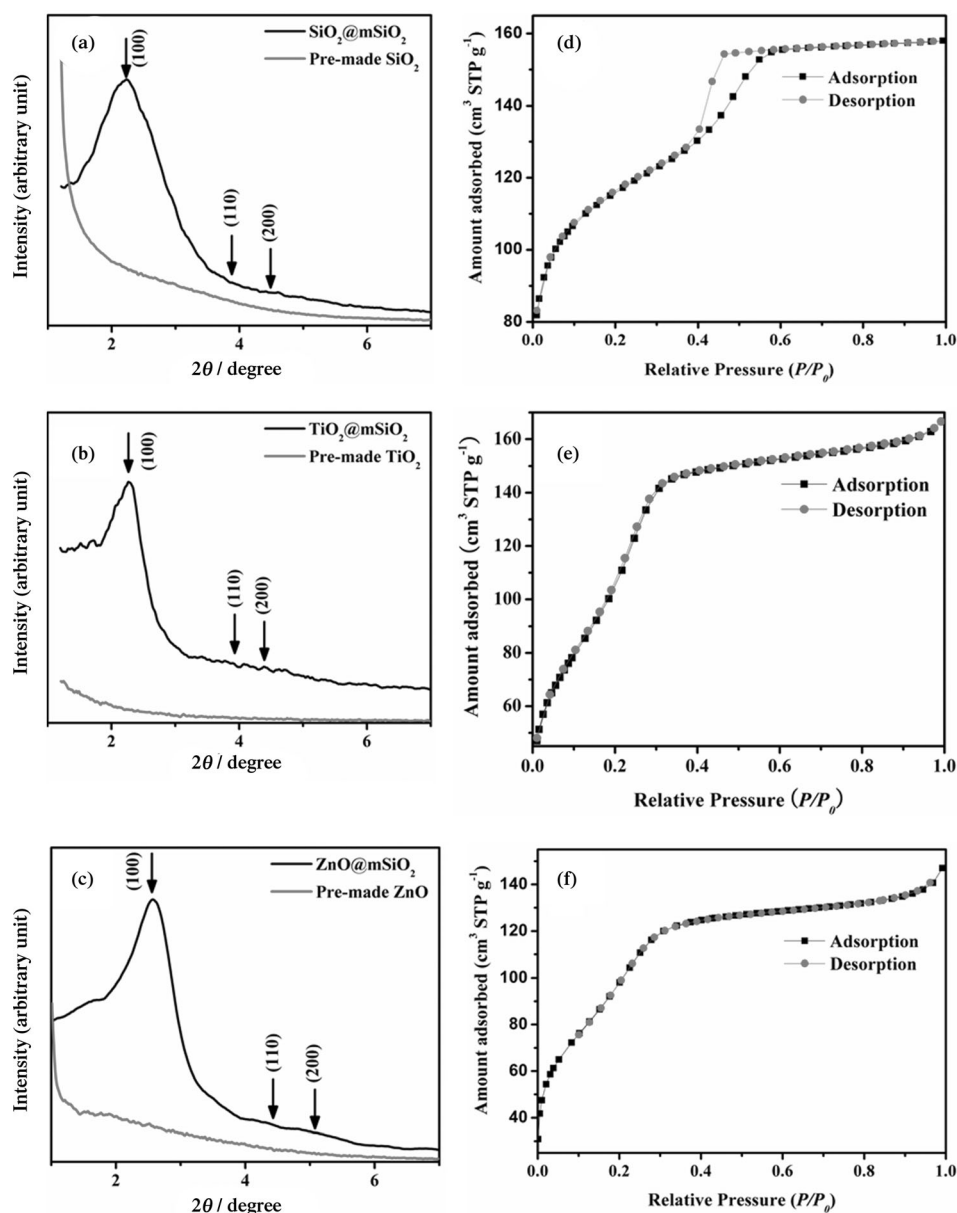
Figure 5. SAXS patterns of a) as-prepared SiO$_2$ and SiO$_2$@mSiO$_2$ particles, b) as-prepared TiO$_2$ and TiO$_2$@mSiO$_2$ particles, and c) as-prepared ZnO and ZnO@mSiO$_2$ particles. N$_2$ adsorption/desorption isotherms of d) SiO$_2$@mSiO$_2$, e) TiO$_2$@mSiO$_2$, and f) ZnO@mSiO$_2$ hybrid particles.

cates the completion of monolayer adsorption and beginning of multilayer adsorption at this point.[30] Together with the TEM observations, the average pore size determined from the adsorption isotherm (BJH method) of the sample was 3.36 nm.

The wall thickness (t) of the meso-layers calculated to be 1.22 nm, by using the relation t = (a$_0$−pore size). The BET surface area and BJH cumulative desorption pore volume for the sample were 428.9 m$^2$g$^{-1}$ and 0.0957 ccg$^{-1}$, respectively. WAXD patterns of the as-prepared TiO$_2$ core particles and the hybrid TiO$_2$@mSiO$_2$ particles are presented in Figure S5 (in the Supporting Information). The one-step calcination process helped to remove the surfactant (CTAB) and to crystallize TiO$_2$ core particles in single anatase phase (JCPDS No. 861157). The SAXS patterns of the as-prepared TiO$_2$ particles and TiO$_2$@mSiO$_2$ particles presented in Figure 5b revealed a first order diffraction peak at about 2.26$^0$ and two higher-order diffraction peaks correspond to the interplanar spacings (d) of 3.90, 2.26 and 1.93 nm, respectively.

Considering the formation of hexagonally ordered structure, the diffraction peaks were matched to the (100), (110) and (200) planes of the mesoporous lattice. The lattice parameter a$_0$ for the meso-lattice in TiO$_2$@mSiO$_2$ particles was calculated to be 4.50 nm from the relation a$_0$ = 2*×$d_{100}$/√3. The average pore size calculated using BJH method was 3.15 nm. The wall thickness was calculated to be 1.35 nm from a$_0$. The BET surface area and BJH desorption pore volume for TiO$_2$@mSiO$_2$ particles were estimated to be 327.2 m$^2$g$^{-1}$ and 0.041 cc g$^{-1}$, respectively. The SAXS pattern of the ZnO@mSiO$_2$ core–shell particles after calcination is shown in Figure 5c. The ZnO@mSiO$_2$ hybrid structures revealed the characteristic SAXS pattern very similar to the TiO$_2$@SiO$_2$ sample with d values of about 3.45, 2.09, and 5.89 nm, indicating a short-range order and hexagonal phase of the mesoporous layer. The unit cell parameter a$_0$ calculated for this case was about 3.98 nm. The

layer. The unstructured higher-order peaks are indicative of short-range-ordered hexagonal structures of the porous layer. Angular positions of the higher order peaks at the √3 and √4 of the first-order diffraction (indicated by arrows) also indicate the formation of hexagonally ordered structures. The diffraction peaks could be indexed as the (100), (110) and (200) planes of the mesoporous lattice. The unit cell parameter a$_0$ for the meso-lattice was calculated to be 4.584 nm using the relation a$_0$ = 2*×$d_{100}$/√3. The N$_2$ adsorption/desorption isotherms of the SiO$_2$@mSiO$_2$ sample (Figure 5 d) revealed a type-IV isotherm according to the IUPAC classification.[30] An abrupt increase in the amount of N$_2$ adsorption from STP to a relative pressure of 0.4 indi-

pore size and BET surface area for the sample were 2.61 nm and 391.78 $m^2g^{-1}$, respectively.

To induce functionalities in the core@$mSiO_2$ structures, several elements were incorporated into their porous shells. In our previous report, we have demonstrated that metal nanoparticles can be organized over the $SiO_2$ nanoparticle surface through the deprotonation of hydroxyl ligands.[26, 28] With partially localized hydroxyl groups at the surface of $mSiO_2$ layer, hetero-element ions approach into their pores. Utilizing this mechanism, we could incorporate Ag, Mn, and Ti ions into the porous network of the $mSiO_2$ shell layers. The formation of Mn, Ag, and $TiO_2$ nanoclusters inside the pores of $mSiO_2$ was probed through their TEM images and elemental mapping. As shown in Figure 6, after incorporation of hetero-element ions, the clear pores of the meso-shells were partially blocked. Homogeneous distribution of Mn, Ag, and $TiO_2$ clusters inside the pore structures of $mSiO_2$ can be clearly seen in the elemental mapping images presented in the Figure 6d, h, and l. Specially, the composite particles with Mn incorporated $mSiO_2$ shells were probed for their free radical and catalytic evaluations (Figure 7). The room temperature X-band electron spin resonance (ESR) spectrum of the Mn-incorporated $mSiO_2$ shell (Figure 7a) exhibits a sextet splitting with a g factor of 2.0085 and an isotropic hyperfine coupling, $A_{iso}$ of 9.7 G, clearly indicating the paramagnetic divalent state of the Mn ions ($I = 5/2$) incorporated into the porous shells.

It is worthy of note that the unpaired electrons of Mn(II) in the $mSiO_2$ shells are well dispersed in the shell framework as paramagnetic guests compared with the non-paramagnetic $mSiO_2$ shell (Figure 7a). It means that incorporation of hetero-element ions is clearly promising for catalytic applications through their host–guest system. Taking into account
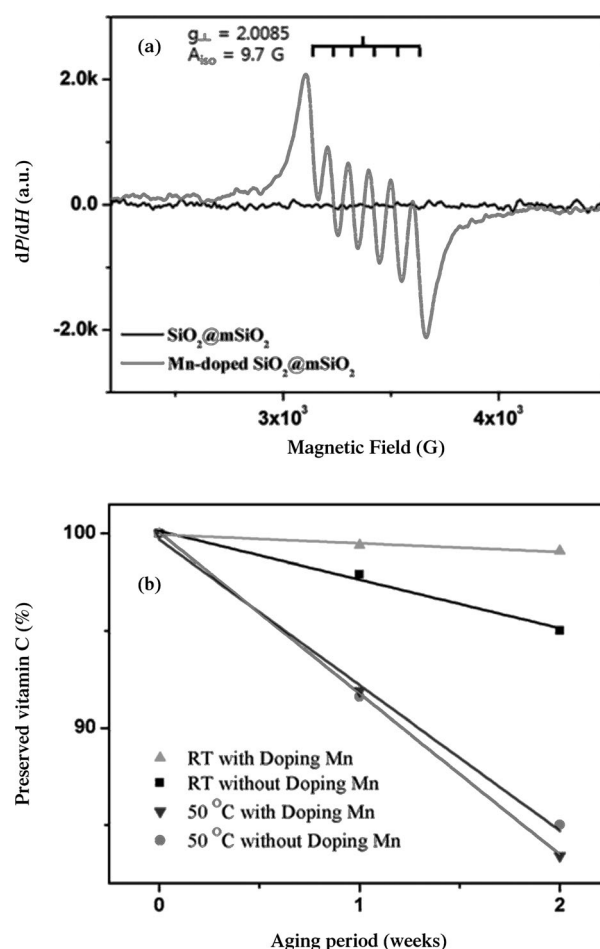


Figure 7. a) X-band ESR spectra of Mn-incorporated $SiO_2$@$mSiO_2$ (gray line) and $SiO_2$@$mSiO_2$ (black line); b) Release of incorporated vitamin C (%) with time for the Mn-doped and undoped $mSiO_2$ at RT and 50 °C.
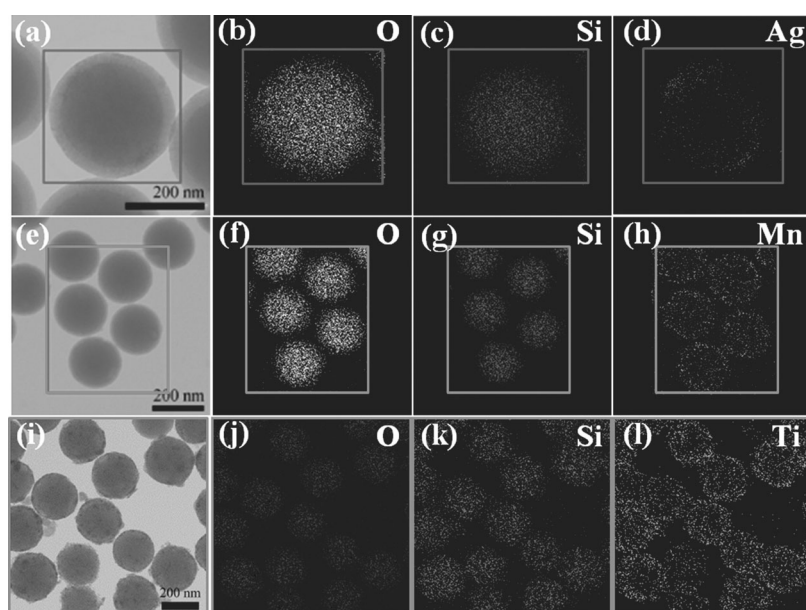


Figure 6. TEM images and EDS mapping results of Ag- (a, b, c, d), Mn- (e, f, g, h) and $TiO_2$- (i, j, k, l) incorporated $SiO_2$@$mSiO_2$ composite particles.

of its TEM and ESR results, the Mn-doped $mSiO_2$ sample was utilized to evaluate its anti-oxidizing effect. The degradation suppression of L-ascorbic acid by free radicals was considered as the estimation of anti-oxidation effect of manganese in the composite. The free-radical scavenging-capacity was measured by preserved L-ascorbic acid % analysis. Figure 7b indicates that a larger amount of L-ascorbic acid could be preserved by the Mn-doped $mSiO_2$ sample for a prolonged time even above room temperature. Over 99 wt% of L-ascorbic acid could be preserved even after two weeks at RT. The wt% of preserved L-ascorbic acid by

the Mn-doped mSiO$_2$ sample is considerably higher than that of the undoped mSiO$_2$ sample, which indicates that the Mn-doped mSiO$_2$ sample has a free-radical-scavenging capacity.

We could test the TiO$_2$ nanocluster-incorporated composite particles for photocatalytic degradation of rhodamine B under UV light. As can be seen from Figure 8, upon UV ir-
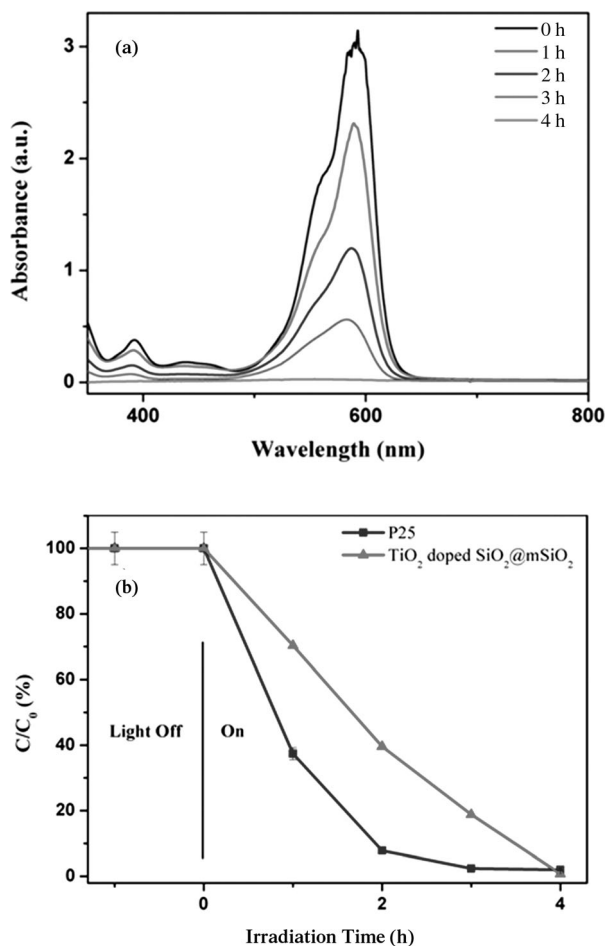


Figure 8. a) Absorption spectra of the rhodamine B solution in the presence of TiO$_2$ cluster-incorporated SiO$_2$@mSiO$_2$ under UV exposure; b) photocatalytic degradation rate of rhodamine B by TiO$_2$ cluster incorporated SiO$_2$@mSiO$_2$ and bare TiO$_2$ nanoparticles (Degusa P25, $\approx$30 nm) under UV irradiation ($\lambda = 300$ nm).

radiation the intensity of the characteristic absorption peak (at 580 nm) of the dye decreases. After about 4 h of UV illumination, the absorption peak almost disappeared. Though the photocatalytic degradation rate for the porous composite particles is a bit slower in comparison with naked/bare TiO$_2$ nanoparticles (Degusa P25 $\approx$30 nm), their difference might be due to the lower amount of TiO$_2$ incorporated into the composite particles. However, with prolonged UV irradiation, the TiO$_2$ nanocluster-incorporated composite particles with a smaller amount of TiO$_2$ have a similar effect (degradation capacity) as Degusa P25 because of their size effect (smaller size). Moreover, the photocatalytic activity of

the composite particles did not decrease even after 10 cycles, indicating their excellent reusability. The composite particles could be collected from the catalytic reaction mixture very easily. The possibility of incorporating several hetero-elemental guest clusters in these mesoporous composite particles makes them highly attractive for multifunctional applications. Whereas Ag cluster-incorporated composite particles can be utilized for the annihilation of bacteria,[28] Mn$^{2+}$-incorporated composite particles have antioxidation properties and could also be utilized in catalytic reactions.

**Conclusion**

Compared with earlier research, this combined approach with core materials and meso-shell is highly promising for the fabrication of multifunctional hybrid structures. Interestingly, various semiconductors, energy conversion materials and catalytic materials can be applied as core material through this facile approach for applications in energy and environmental fields. In summary, hybrid M@mSiO$_2$ and MO@mSiO$_2$ nanotructures of different core and shell dimensions could be fabricated on pre-synthesized metal or metal oxide nanoparticles. The three-step fabrication process consists of synthesizing metal- or metal oxide nanoparticles through a wet chemical process, interaction of SDA micelle with the core particle surface, and formation of the final hybrid structure on removing the SDA through calcinations. The homogeneity of the meso-shells and the final morphology of the hybrid particles depend strongly on the dispersion ability of the core particles and their pH stability. Our three-step strategy can be extended to fabricate spherical particles of more complex structures. Moreover, the outward oriented channels of the meso-silica shells make these hybrid structures attractive for multi-functional applications by introducing suitable guest molecules in their oriented pores. Whereas the guest molecule-incorporated mSiO$_2$ shells are promising for applications in the anti-aging or anti-wrinkling cosmetics, they can also act as effective catalysts and photocatalysts for the degradation of organic molecules.

**Experimental Section**

**Sol–gel synthesis of solid SiO$_2$ core particles**: SiO$_2$ nanoparticles were synthesized according to our reported method.[26] The size of SiO$_2$ nanoparticles was controlled by adjusting the molar ratio of TEOS, water, and ammonia solution.[14] For example, silica nanoparticles of approximately

95 nm in diameter were synthesized through hydrolysis and condensation of TEOS (0.125 mol, 28 mL) in a mixture of ethanol (4.28 mol, 250 mL), water (0.25 mol, 4.5 mL), and ammonia solution (0.25 mol, 4.78 mL).[26] For the synthesis of silica particles of about 130 nm diameter, instead of 0.25 mL ammonia in the earlier recipe, about 0.375 mol (71.7 mL) of ammonia solution was utilized.[28] Silica particles with a diameter of 320 nm were synthesized using 0.45 mol (20 mL) of water and 2.1 mol (10 mL) of ammonia solution. For all the samples, the reactions were performed at room temperature (RT) under vigorous magnetic agitation for 6 h.

**Sol–gel synthesis of TiO$_2$ particles**: The titania spheres were synthesized according to the reported procedure with some modifications.[31] First, Ti-(OBu)$_4$ (1 mL) was added to ethylene glycol (25 mL). The mixture was magnetically stirred for 12 h at RT to form titanium glycolate. This stable precursor was then added dropwise into acetone (100 mL, 0.3% water content) under agitation. After about 30 min of agitation the mixture was left to stand for 6 h. The product was separated by centrifuging, washed with ethanol, and dried in atmospheric ambient.

**Fabrication of mesoporous SiO$_2$ shell over SiO$_2$ cores (SiO$_2$@mSiO$_2$)**: For the fabrication of SiO$_2$@mSiO$_2$ structures, we used the same strategy as reported by Botella et al.[32] with some modifications. First a pre-fabricated silica sol (10 mL) was diluted by adding water/ethanol (20 mL, 1:1, v/v) mixture under agitation. Ethanol was introduced as co-solvent both for a better dispersion of the pre-fabricated SiO$_2$ cores and to control the meso-silica shell width. To the earlier solution, water/ethanol mixture (600 mL, 20:1, v/v) and 0.008 mol (3 g) of CTAB were added under magnetic stirring for 30 min. Then, TEOS (6 mL, 0.027 mol) was added to the solution under magnetic stirring. The pH of the reaction mixture was controlled in between 10 and 11 by the addition of ammonia solution. The final solution was kept under magnetic stirring for 24 h. After 24 h of agitation, the product was collected by centrifuging and washing with ethanol. The dried product was calcined at 600 °C for 5 h.

**Fabrication of mesoporous SiO$_2$ shell over TiO$_2$ cores (TiO$_2$@mSiO$_2$)**: 0.125 mol (10 g) of pre-fabricated TiO$_2$ powder was dispersed to a water/ethanol mixture (900 mL, 2:1, v/v). This TiO$_2$ sol was used to fabricate meso-silica shell over TiO$_2$ particles. For the growth of the meso-silica shell, we used the same procedure as in the case of SiO$_2$@mSiO$_2$ structures described in the previous section.

**Incorporation of Mn, Ag, and TiO$_2$ nanoparticles in meso-SiO$_2$ shell**: For the incorporation of Mn in porous core–shell structures, first MnCl$_2$·4H$_2$O (0.3 g) was dissolved in ethanol (10 mL) and water mixture (v/v = 7:3). The previously synthesized SiO$_2$@mSiO$_2$ (0.03 g) was then added to this solution. The mixture was kept under ultrasonic agitation for 30 min in an ice bath. The ultrasonic treatment was repeated three times, after which the sample was washed several times by ethanol and water, and dried in air at 90 °C. For the incorporation of Ag, the same procedure was utilized.

For the incorporation of TiO$_2$, we followed the procedure reported by Xia et al.[33] Typically, titanium(IV) butoxide (about 0.05 mL) was added into ethylene glycol (10 mL) containing prefabricated SiO$_2$@mSiO$_2$ (0.03 g) at room temperature under magnetic agitation. After aging the mixture for 6 h at room temperature, it was added dropwise into acetone under magnetic agitation. After about 10 min of agitation, the sample was washed repeatedly by ethanol, dried in air at 90 °C and then air annealed at 500 °C for 2 h.

**Characterization**: For morphology and structural characterization of the samples a JEOL, JEM 2100F field emission transmission electron microscope (FETEM) attached with 2k X 2k Charge Coupled Device, scanning transmission electron microscopy, and energy dispersive spectroscopy system was utilized. For transmission electron microscopic (TEM) observations, the samples were prepared by placing one drop of the colloidal solution onto carbon-coated copper grids of 200 mesh size and dried under an IR lamp for few minutes. The particle size and pore size of the MO@mSiO$_2$ structures were evaluated using their TEM micrographs. To determine the crystallinity and crystal structure of the synthesized samples, a Rigaku D′Max 2200 V (Cu$_{K\alpha}$ radiation, $\lambda = 1.5406$ Å) wide-angle X-ray diffraction system, and a Rigaku D′Max 2500 18 K small-angle X-ray scattering system were utilized. For the N$_2$ adsorption/desorption iso-

therms, an automated QUADRASORB "SI" analyzer of Quantachrome Instruments was used.

**Electron spin resonance (ESR) measurement and Catalytic test**: For ESR spectra of meso SiO$_2$ shell with manganese was recorded on JEOL (JAPAN), JES PX 2300 FT-ESR with 1.4 T electromagnet and 8800–9600 MHz output frequency(X-band) at Pukyong National University, Korea. Test of antioxidizing effect of manganese was carried with Research Center in The Face Shop LTD, Korea. The photocatalytic activity was monitored during photo-degradation of organic dye, rhodamine B at RT, and compared with the activity of commercial titania, Degussa P25. Photocatalytic degradation was carried out in a 50 mL glass vial. The aqueous slurry (30 mL) with 15 mg of Degussa P25 and rhodamine B was aged in the dark for 30 min for the dye to be adsorbed on the surface of TiO$_2$. A 300 W Xe lamp (ARC research sce MODEL 66984, USA) was placed above the reaction slurry. The degradation of dye with ultraviolet irradiation time was monitored in a UV/VIS (Model: Jasco V-600 series) spectrophotometer at RT and an average value was obtained from three measurements.

# Acknowledgements

[1] C. T. Kresge, M. E. Leonowicz, W. J. Roth, J. C. Vartili, J. S. Beck, *Nature* **1992**, *359*, 710.

[2] S. Angloher, J. Kecht, T. Bein, *Chem. Mater.* **2007**, *19*, 3568.

[3] D. Baute, H. Zimmermann, S. Kababya, S. Vega, D. Goldfarb, *Chem. Mater.* **2005**, *17*, 3723.

[4] L. Han, O. Terasaki, S. Che, *J. Mater. Chem.* **2011**, *21*, 11033.

[5] a) A. Corma, *Chem. Rev.* **1997**, *97*, 2373; b) M. Shakeri, C.-W. Tai, E. Gcthelid, S. Oscarsson, Jan-E. Backvall, *Chem. Eur. J.* **2011**, *17*, 13269; c) S. Okada, K. Mori, T. Kamegawa, M. Che, H. Yamashita, *Chem. Eur. J.* **2011**, *17*, 9047.

[6] N. Suzuki, S. Kiba, Y. Kamachi, N. Miyamoto, Y. Yamauchi, *J. Mater. Chem.* **2011**, *21*, 5338.

[7] A. Yan, T. Dein, *Chem. Mater.* **1992**, *4*, 975.

[8] R. Zhang, W. Ding, B. Tu, D. Zhao, *Chem. Mater.* **2007**, *19*, 4379.

[9] J. E. Lee, D. J. Lee, N. Lee, B. H. Kim, S. H. Choi, T. Hyeon, *J. Mater. Chem.* **2011**, *21*, 16869.

[10] Y. Wan, D. Zhao, *Chem. Rev.* **2007**, *107*, 2821.

[11] S. H. Joo, J. Y. Park, C.-K. Tsung, Y. Yamada, P. Yang, G. A. Somorjai, *Nat. Mater.* **2009**, *8*, 126.

[12] S. Mintova, S. Y. Mo, T. Bein, *Chem. Mater.* **2001**, *13*, 901.

[13] a) A. l-Noriega, E. R-Hernandez, S. M. Stevens, D. Arcros, M. W. Anderson, O. Terasaki, M. Vallet-Regi, *Chem. Mater.* **2009**, *21*, 18; b) J. Sun, X. Bao, *Chem. Eur. J.* **2008**, *14*, 7478.

[14] W. Stöber, A. Fink, E. Bohn, *J. Colloid Interface Sci.* **1968**, *26*, 62.

[15] Y. Deng, D. Qi, C. Deng, X. Zhang, D. Zhao, *J. Am. Chem. Soc.* **2008**, *130*, 28.

[16] S. B. Yoon, J.-Y. Kim, J. H. Kim, Y. J. Park, K. R. Yoon, S.-K. Park, J.-S. Yu, *J. Mater. Chem.* **2007**, *17*, 1758.

[17] K. R. Lee, S. Kim, D. H. Kang, J. I. Lee, Y. J. Lee, W. S. Kim, D. H. Cho, H. B. Lim, J. Kim, N. H. Hur, *Chem. Mater.* **2008**, *20*, 6738.

[18] M. E. Davis, *Nature* **2002**, *417*, 813.

[19] W. Zhao, J. Gu, L. Zhang, H. Chen, J. Shi, *J. Am. Chem. Soc.* **2005**, *127*, 8916.

[20] J. Kim, J. E. Lee, J. Lee, J. H. Yu, B. C. Kim, K. An, Y. Hwang, C.-H. Shin, J.-G. Park, J. Kim, T. Hyeon, *J. Am. Chem. Soc.* **2006**, *128*, 688.

[21] F. Jiao, H. Frei, *Energy Environ. Sci.* **2010**, *3*, 1018.

[22] Z. Zhu, X. Xie, S. A. C. Carabineiro, P. B. Tavares, J. L. Figueiredo, R. Schomacker, A. Thomas, *Energy Environ. Sci.* **2011**, *4*, 2020.

[23] R. T. Koodali, D. Zhao, *Energy Environ. Sci.* **2010**, *3*, 608.

[24] Y. Li, X. L. Zhang, R. Qiu, R. Qiao, Y. S. Kang, *J. Phys. Chem. C* **2007**, *111*, 10747.

[25] R. Strobel, H. J. Metz, S. E. Pratsinis, *Chem. Mater.* **2008**, *20*, 6346.

[26] Y. H. Kim, D. K. Lee, H. G. Cha, C. W. Kim, Y. C. Kang, Y. S. Kang, *J. Phys. Chem. B* **2006**, *110*, 24923.

[27] M. Ye, Q. Zhang, Y. Hu, J. Ge, Z. Lu, L. He, Z. Chen, Y. Yin, *Chem. Eur. J.* **2010**, *16*, 6243.

[28] Y. H. Kim, D. K. Lee, H. G. Cha, C. W. Kim, Y. S. Kang, *J. Phys. Chem. C* **2007**, *111*, 3629.

[29] a) V. I. Prvulescu, V. Parvulescu, U. Endruschat, G. Filoti, F. E. Wagner, C. Kubel, R. Richards, *Chem. Eur. J.* **2006**, *12*, 2343; b) Y. Lu, Y. Yin, B. T. Mayer, Y. Xia, *Nano Lett.* **2002**, *2*, 183; c) X. Li, V. T. John, J. Zhan, G. He, L. Spinu, *Langmuir* **2011**, *27*, 6252.

[30] K. S. W. Sing, D. H. Everett, R. A. W. Haul, L. Moscou, R. A. Pierotty, J. Rouquerol, T. Siemieniewska, *Pure Appl. Chem.* **1985**, *57*, 603.

[31] M. Pal, J. García Serrano, P. Santiago, U. Pal, *J. Phys. Chem. C* **2007**, *111*, 96.

[32] P. Botella, A. Corma, T. M. Navarro, *Chem. Mater.* **2007**, *19*, 1979.

[33] X. Jiang, T. Herricks, Y. Xia, *Adv. Mater.* **2003**, *15*, 1205.